NOTATION

X, the longitudinal coordinate, mm; d_{eq}, the equivalent diameter of the channel flow-through section, mm; δ, the thickness of the secondary boundary layer, mm; D, the diameter of the face flange, mm; R, the curvature radius of the inlet edge, mm; B, the barometric pressure, Pa; p_{st}, the surface static pressure, Pa; T_{flow}, the temperature of the air that is drawn in, K; $Re_{d_{eq}}$, the Reynolds number calculated on the basis of the average flow rate. Indices: 2, 3, 4, section number; max, maximum; flow, flow.

LITERATURE CITED

1. V. M. Legkii and V. A. Rogachev, Inzh.-Fiz. Zh., 56, No. 2, 215-220 (1980).
2. V. D. Burlei, "Investigating the exchange of heat and flow in the initial segments of circular tubes," Dissertation, Candidate of Technical Sciences, Kiev (1982).
3. A. S. Makarov, "Certain quantitative relationships governing the flow and transfer of heat in the initial segments of rectangular channels," Dissertation, Candidate of Technical Sciences, Kiev (1970).
4. E. M. Sparrow and N. Kern, Teploperedacha, 105, No. 3, 100-109 (1983).
5. E. M. Sparrow and N. Kern, Teploperedacha, 104, No. 1, 89-97 (1982).
6. V. M. Legkii and V. D. Burlei, Prom. Teplotekhn., 7, No. 1, 6-9 (1985).

APPLICATION OF THE LARGE-SCALE PARTICLE METHOD IN INVESTIGATING THE EXCHANGE OF HEAT BETWEEN A GAS AND PARTICLES IN TWISTED-FLOW COUNTERCURRENT APPARATUS

É. F. Shurgal'skii

UDC 532.529

The model of interpenetrating continua serves as the basis for an investigation into the exchange of heat between a carrier and dispersion phase. It is demonstrated that the exchange of heat increases the efficiency with which dust is collected in vortex-type equipment.

Twisted-flow countercurrent dust collectors (TCDC) occupy a unique place in the technology of dust collection. These collectors are characterized by a high level of dispersed impurity removal from the gases, as well as by their limited sensitivity in purification efficiency to oscillations in the flow rates of the gas and particles at the inlet sections, by the absence of abrasive wear on the inside surfaces of the equipment, etc. In this connection, such equipment is presently being introduced on a broad scale into various branches of industry.

The hydrodynamics of gas suspensions in TCDC has been studied rather fully in [1, 2]. Here, as in many other references, it is assumed that the temperature of the gas and of the particles at the inlet to the equipment is identical. However, in many industrial lines, primarily in those in which the dispersion phase is dried with a hot gas, the temperatures of the gas and of the particles at the inlet to the TCDC will differ significantly, and this difference may bring about a change in the structure of flow interaction within the apparatus as a consequence of heat exchange between the phases.

1. Formulation of the Problem. Let us examine the interaction of two twisted flows in a cylindrical area whose longitudinal cross section can be seen in Fig. 1. In this figure AL denotes the axis of symmetry, while the lines BCDE and MN identify the solid walls. A preliminary twisted flow, containing the particles of the dispersion phase, is passed through the section AB. At the other end, through the circular section ME, we have the secondary

Moscow Chemical Machine-Building Institute. Translated from Inzhenerno-Fizicheskii Zhurnal, Vol. 56, No. 4, pp. 550-555, April, 1989. Original article submitted April 25, 1988.

0022-0841/89/5604-0384$12.50

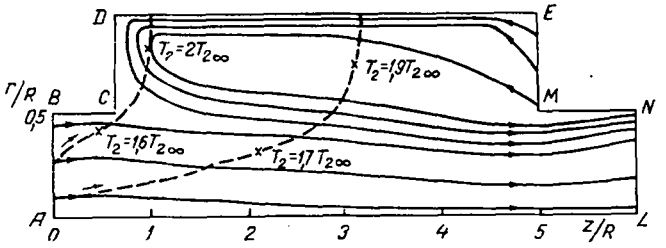

Fig. 1. Projections of the phase streamlines onto the longitudinal cross section of a channel.

twisted flow without any particles (this is the situation in a number of dust collectors in which the secondary flow is supplied through a nozzle). The equations which describe this problem within the scope of a two-velocity two-temperature model of a two-phase medium have the form [3]:

$$\frac{\partial \rho_i}{\partial t} + \operatorname{div}(\rho_i \mathbf{v}_i) = 0,$$

$$\frac{\partial \rho_i \mathbf{v}_i}{\partial t} + \sum_k \nabla^k \rho_i v_i^k \mathbf{v}_i = (i-2)\nabla p - \mathbf{f}_{ij},$$

$$\frac{\partial}{\partial t}(\rho_1 E_1 + \rho_2 E_2) + \operatorname{div}(\rho_1 E_1 \mathbf{v}_1 + \rho_2 E_2 \mathbf{v}_2) + \operatorname{div}(p\mathbf{v}_1) = 0$$

$$(E_i = e_i + 1/2\mathbf{v}_i^2), \tag{1}$$

$$\frac{\partial \rho_2 e_2}{\partial t} + \sum_k \nabla^k \rho_2 e_2 v_2^k = q_{12},$$

$$p = \rho_1^0(\gamma - 1)e_1, \quad e_1 = c_{v1}T_1, \quad e_2 = c_2 T_2, \quad \rho_2^0 = \text{const},$$

$$\mathbf{f}_{ij} = \frac{n}{8}\pi d^2 C_d \rho_1^0 (\mathbf{v}_1 - \mathbf{v}_2)|\mathbf{v}_1 - \mathbf{v}_2|,$$

$$q_{12} = \pi n d \lambda_1 \operatorname{Nu}(T_1 - T_2).$$

For the coefficient of aerodynamic drag C_d of the particles and for the Nusselt number Nu we will assume the following relationship:

$$C_d = \frac{24}{\mathrm{Re}_{12}} + \frac{4}{\sqrt{\mathrm{Re}_{12}}} + 0.4, \quad \mathrm{Pr} = \frac{c_p \mu_1}{\lambda_1},$$

$$\mathrm{Nu} = 2 + 0.6\,\mathrm{Re}_{12}^{1/2}\,\mathrm{Pr}^{1/3}, \quad \mathrm{Re}_{12} = \frac{\rho_1^0 |\mathbf{v}_1 - \mathbf{v}_2| d}{\mu_1}. \tag{2}$$

The boundary conditions for system of equations (1) were established as follows: at the solid walls BCDE, MN the condition of nonpenetration for the gas and the condition of an absence of reflection for the particles (it is assumed that the particles entering the side surface disappear from the apparatus); at the right outer boundary NL the condition of flow uniformity along the axial coordinate, i.e., the derivatives were assumed to be zero along the normal to the calculated region from the flow parameters; the primary and secondary flows were given, respectively, at the boundaries AB and ME; at the axis of symmetry AL of the apparatus we have the condition of flow symmetry. The original system of equations was made dimensionless, and the characteristic quantities were the parameters of the gas in the section AB and the radius R of the apparatus. The following parameters are most essential for this type of problem: mass particle concentration in the primary flow $r_{2\infty} = \rho_{2\infty}/\rho_{1\infty}{}^0$; and the parameters characterizing the nonequilibrium of the velocity phase $\beta^{(v)}$ and the thermal phase $\beta^{(\tau)}$:

$$\beta^{(v)} = \frac{\rho_2^0 d^2 v_{1\infty}}{18\mu_1 R}, \quad \beta^{(\tau)} = \frac{c_2 \rho_2^0 d^2 v_{1\infty}}{12\lambda_1 R};$$

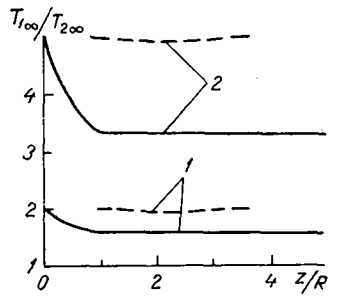

Fig. 2

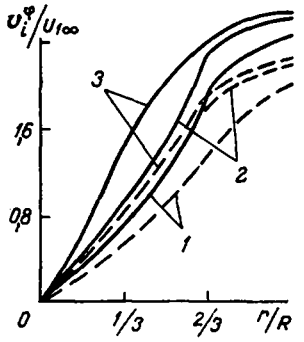

Fig. 3

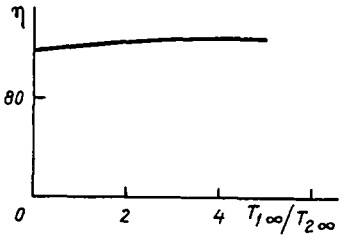

Fig. 4

Fig. 2. Distribution of gas temperature along the axis of symmetry and the side wall: 1) $T_{1\infty} = 2T_{2\infty}$; 2) $T_{1\infty} = 5T_{2\infty}$.

Fig. 3. Distribution of tangential gas-velocity component (solid curves) and of the particles (dashed lines) in the section z = 3R: 1) $T_{1\infty} = T_{2\infty}$; 2) $T_{1\infty} = 2T_{2\infty}$; 3) $T_{1\infty} = 5T_{2\infty}$.

Fig. 4. Gas purification efficiency as a function of the phase temperature drop across the section AB. η, %.

the Reynolds number calculated on the basis of particle dimension $Re_d = \rho_{1\infty}{}^0 v_{1\infty} d/\mu_1$, the Mach number M_∞ of the primary flow, the components of the gas velocity vector in the sections AB and ME (it was assumed that at AB the gas velocity vectors and those of the particles coincide); the heat-capacity ratio cv_1/c_2 and the ratio $T_{1\infty}/T_{2\infty}$ of the absolute gas and particle temperatures at the inlet to the apparatus, as well as the geometric parameters characterizing the region, are shown in Fig. 1.

2. Numerical Integration Scheme. We used the large-scale particle method [4] as modified in [5] for the movement of a gas at low subsonic speeds ($M_\infty \leq 0.1$) for the numerical integration of the system (1). We employed a first-order accuracy scheme. The accuracy was monitored by comparing the numerical solutions obtained in grids of 74 × 14 and 74 × 28, and the doubling of the number of cells was carried out in the direction of the higher values of the flow gradient parameters. In each of the variants the difference in the results did not exceed 3-5%. Moreover, we used the results obtained to analyze the magnitude of the schematic viscosity by resorting to the parabolic form of the first differential approximation of the difference scheme employed. The analysis demonstrated that the contribution of the terms containing the schematic viscosity is negligibly small in comparison with the contribution of the turns in the right-hand sides of Eqs. (1) virtually throughout the entire region of the flow, and we have reference here, for example, to the pressure gradient or the force of interphase interaction. Just as in the conventionally large-scale particle method, the intermediate values of the gas phase alone are calculated in the Euler stage. The dispersion-phase parameters remain constant in this stage, since the pressure gradient is not included in the equations for the solid phase. The transfers of mass, momentum, and energy for each phase through the boundaries of the cell are calculated in the Lagrange stage. In the concluding stage, based on the laws of the conservation of mass, momentum, and energy, we find the values of the phase parameters at a new temporal layer. Here we take into con-

sideration the force interaction f_{12} and the thermal interaction q_{12}. As is the case with the conventional large-scale particle method scheme, the solid-phase parameters are calculated algorithmically at the beginning. The dimensionless integration intervals over the three-dimensional coordinates h and over time τ were, respectively, chosen as h = 1/12 and τ = 0.1h. The calculations were carried out for various values of the determining parameters and the geometric dimensions of the region.

3. Results of Calculations. We now present the results from the solution of the problem for $M_\infty = 0{,}08$, $r_{2\infty} = 1$, $\beta^{(v)} = 0{,}007$, $\beta^{(\tau)} = 0{,}006$, $v_{1w}^z/v_{1\infty}^z = -0{,}5$, $v_{1w}^\varphi/v_{1\infty}^z = 3{,}6\,(r - 0{,}5R)/R$, $v_{1\infty}^\varphi/v_{1\infty}^z = 3{,}6r/R$, $T_{1\infty}/T_{2\infty} = 2;\ 5$, $v_{1\infty}^r = v_{2\infty}^r = v_{1w}^r = v_{1w} = 0$, $T_{1w} = T_{1\infty}$.

The relationships between the geometric dimensions of the apparatus were chosen as follows: DC = AB, BC = AB, DE = 4AB, MN = AB, ME = AB, NL = AB.

Figure 1 shows the projections of the phase streamlines onto the longitudinal cross section of the channels (the solid lines represent the gas and the dashed lines represent the particles, $T_{1\infty}/T_{2\infty} = 2$), and the flow pattern for the gas phase has the following appearance: the secondary flow, entering the channel from section ME, extending to the boundary CD, executes a turn and together with the dust-filled primary flow, which is supplied to the apparatus from AB, moves in the direction of the outlet section. We see from Fig. 1 that in TCDC with a large dispersion phase the boundary of separation between the primary and secondary flows is not parallel to the side surface of the apparatus. This is associated with the fact that the force and thermal interactions of the phases leads to a redistribution of pressure within the apparatus, as a consequence of which there is a significant change in the flow pattern. Near the point at which the secondary flow changes direction because of the force interaction of the gas and the particles in the tangential direction, we have an expansion of the primary flow and a compression of the secondary flow. At a distance on the order of 2-3R from the inlet section AB, because of the intensive exchange of heat between the phases, the hot gas of the primary gas is cooled, resulting in its compression and in the expansion of the secondary flow. Figure 1 shows the values of the particle temperatures at the points noted on the streamlines of the dispersion phase by crosses. We can see that the particle temperature attains its maximum value, virtually equal to $T_{1\infty}$, within the zone in which the secondary flow is moving.

Figure 2 shows the distributions of the gas temperature along the axis of symmetry (solid lines) and along the side wall (dashed lines). The figure shows that at a distance on the order of R from the inlet section AB there occurs a sharp drop in the temperature of the gas because of the intensive removal of heat to the particle. The particle temperature is elevated in this segment and for the case in which z > R the gas temperature and that of the particles evens out. We can see from the figure that the temperature of the gas at the wall is considerably higher than the temperature of the gas at the axis of symmetry because the concentration of particles within the apparatus diminishes from the center toward the periphery, and at the same time we see that there is a reduction in the exchange of heat between the gas and the particles. It should also be noted that the gas-temperature profile at the wall exhibits a somewhat nonmonotonic nature because of the fact that some accumulation of particles occurs near BC.

We can see from Fig. 3 that the tangential velocity, both of the gas and of the particles, increases markedly with an increase in the temperature difference across the inlet cross section (particularly in the region r/R < 2/3), and there is a more intensive interaction between the primary and secondary flows. This leads to an increase in the efficiency η of gas purification (Fig. 4).

These calculations show that the large-scale particle method may be used effectively to simulate processes of interphase heat exchange in equipment in which the gasdynamic processes are exceedingly complex.

NOTATION

ρ, the reduced density; v, the velocity vector; p, the pressure in the gas; E, the total gas energy; e, the internal energy; T, temperature; n, the number of particles per unit volume; γ, the index of the adiabatic curve of the gas; c_{v1}, the specific heat capacity of the gas at constant volume; c_2, the specific heat capacity of the particles; c_{p1}, the specific heat capacity at constant pressure; μ_1, the coefficient of dynamic gas viscosity; λ_1, the coefficient of gas thermal conductivity; f_{12}, the force of friction between the phases; q_{12},

the intensity of heat exchange between the phases; C_d, the coefficient of particle aerodynamic drag; Nu, Nusselt number; Re_{12}, Reynolds number for the streamlining of the particles; Pr, Prandtl number; d, the particle diameter; R, the radius of the apparatus. Subscripts: i = 1, gas; i = 2, particles; k, the summation index; ∞, the parameters have been taken at the section AB; w, indicates that the parameters have been taken at the section ME; r, φ, z, the axes of the cylindrical coordinate system.

LITERATURE CITED

1. V. D. Goryachev, V. V. Chernyshev, and R. P. Kornev, Izv. Vyssh. Uchebn. Zaved., Énergetika, No. 3, 67-72 (1984).
2. B. S. Sazhin, B. P. Lukachevskii, M. Sh. Dzhunisbekov, et al., Teor. Osnovy Khim. Tekhnol., 19, No. 5, 687-690 (1985).
3. R. I. Nigmatullin, The Fundamentals of the Mechanics of Heterogeneous Media [in Russian], Moscow (1978).
4. O. M. Belotserkovskii and Yu. M. Davydov, The Method of Large-Scale Particles in Gasdynamics. Experimental Calculations [in Russian], Moscow (1982).
5. É. F. Shurgal'skii, Inzh.-Fiz. Zh., 49, No. 1, 51-57 (1985).

ISOTHERMAL AXISYMMETRIC FLOW OF AN INCOMPRESSIBLE FLUID IN RADIAL CONTACT APPARATUS

P. G. Shtern, E. A. Rudenchik, S. V. Turuntaev, I. S. Luk'yanenko, E. G. Bezrukova, and E. K. Popov

UDC 552.546

A method is proposed for the calculation of the axisymmetric flow of an incompressible fluid in a radial apparatus with a nonmoving layer of granular material. An engineering method is developed to evaluate the degree of flow nonuniformity in equipment of this type, thus making it possible operationally to choose among structural solutions in the design of this equipment.

A number of research studies [1-4] have been devoted to the theoretical and experimental study of flow distributions in perforated channels and radial reactors. The energy approach within the framework of a one-dimensional model is utilized in calculating the distributions of flows in perforated channels [1, 2]. The flow model for radial equipment with a nonmoving granular layer, such as that proposed in [3], is valid for low velocities when the resistance to the flow within the catalyst layer depends linearly on the rate of filtration. There is no doubt as to the importance of calculating the flow in industrial reactors, where the quadratic relationship between the pressure drop across the layer and velocity is valid.

Let us examine the axisymmetric flow of an incompressible fluid in an apparatus whose diagram is shown in Fig. 1a. The granular layer is situated between two coaxial perforated cylinders. The fluid flows into the apparatus at a velocity v_{in} through a distributing collector I, passes through to the operating zone III, and is discharged from the apparatus through the outside collector II at a velocity v_{out}. The following circuits may be regarded as special cases: a perforated channel with a dead end (zone I); an apparatus in which the atmosphere functions as zone II (zones I and III).

The mathematical model is based on the assumption that the fluid is incompressible:

$$\operatorname{div} \mathbf{v} = 0, \tag{1}$$

Synthetic Rubber Monomer Scientific-Research Institute, Yaroslavl'. Translated from Inzhenerno-Fizicheskii Zhurnal, Vol. 56, No. 4, pp. 555-562, April, 1989. Original article submitted September 16, 1987.

0022-0841/89/5604-0388$12.50